ATTITUDE CONTROL SYSTEM OF UNDERWATER INTELLIGENT INSPECTION VEHICLE

Jian ZHANG[1], Xiaoyang ZHENG[2], Dongyao GUO[3], Xuhao WANG[4], Zhixin GU[5,*]

Underwater intelligent inspection robot plays an important role in civil and military fields. This paper presents an attitude control system of underwater intelligent inspection robot, which adaptively adjusts its attitude and makes it drive safely in the target direction. A hardware system based on STM32 composed of a posture sensor with positioning function, a pressure sensor and a machine vision circuit board is designed. A fuzzy PID algorithm combined with visual recognition is used, which allows the robot to adjust its posture in real time underwater to achieve precise operations. Experiments show that the attitude control system using the combination of software and hardware reduces the lateral and longitudinal attitude angle errors over 50% in the moving state and over 30% in the static suspension state compared with the traditional scheme.

Keyword: underwater vehicle; PID control; fuzzy PID control; visual identity

1. Introduction

Conventional underwater inspections are conducted by using cable-less underwater robots (AUV) for mass underwater scanning, and then human operated cable-controlled underwater robots (ROV) for targeted removal and recovery [1] of foreign objects. The fully automated intelligent inspection by AUV can save a lot

[1] Engineer, Engineering Teaching Practice Center, Northeast Forestry University, Harbin 150040, China, E-mail: endlesszhang@nefu.edu.cn;
[2] Bachelor, College of Information and Computer Engineering, Northeast Forestry University, Harbin 150040, China, E-mail: 591311968@qq.com
[3] Bachelor, College of Information and Computer Engineering, Northeast Forestry University, Harbin 150040, China, E-mail: 2508694025@qq.com
[4] Bachelor, College of Information and Computer Engineering, Northeast Forestry University, Harbin 150040, China, E-mail: 805105933@qq.com
[5,*] Corresponding author: Zhixin Gu, Associate Professor, College of Information and Computer Engineering, Northeast Forestry University, Harbin 150040, China, E-mail: gzx@nefu.edu.cn

of manpower and resources in practical application, and the key issue of AUV is to adjust the attitude autonomously and operate accurately.

The United States has always been a leader in the field of underwater robotics, and its Remote Environmental Monitoring Units (REMUS) series of AUV, which is a representative AUV developed by Hydroid. The control method is to obtain some hydrodynamic coefficients firstly based on empirical data, then to build the dynamic model of the underwater robot "REMUS", and then to realize its control by linear control method [2], which was developed by Prestero et al. The University of Tokyo, Japan have been developed the "Tam-Egg", "Twin-Burger 1", "Twin-Burger 2", "PTER0A150" and "PTER0A250" and other models of observational autonomous underwater robots [1], which autonomous movement of the robot are realized by adaptive control [3]. The National Center in Southampton, UK, designed the "Autosub" series of AUVs and successfully carried out more than 200 marine scientific investigation missions [4]. The "r2D4" AUV developed by the University of Tokyo, Japan, based on the "R-one" AUV platform, is equipped with a variety of sensors and plays an important role [5] in the observation of 3-dimensional seafloor topography and scientific investigation of hydrothermal vent areas.

China started to develop AUV system platform in the 1990s, and has developed a series of AUV products after more than 30 years of dedicated research. The research institutes represented by Shenyang Institute of Automation of Chinese Academy of Sciences, 710 Research Institute of CSIC, Harbin Engineering University, etc. are the early research units of AUV system in China. The representative ones are the "Submarine Dragon" series of submersibles. The "Submersible Dragon No.1" AUV is the first practical deep-sea AUV in China, with a diving depth of 6000m, and has undertaken the detection of polymetallic nodules since 2013, which is a mature equipment for China's marine research vessels. The "Submersible Dragon No.2" AUV is optimized on the basis of "Submersible Dragon No.1" AUV, with a non-swivel body vertical flat hydrodynamic shape, which aims to adapt the AUV to the needs of complex terrain operations in the hydrothermal zone of the southwest Indian Ocean. The domestic Weifang University team conducted kinematics analysis and simulation for the field of deep-sea mining robots, and obtained the simulation curve of the dynamic characteristics of the robot, which provided a theoretical reference for the research on the kinematics of deep-sea mining robots [6].

Due to the special underwater working environment, which is disturbed by many uncertain factors such as water resistance, viscous force, rotational force, and coupling force of the environmental water body, the motion control model is difficult to establish accurately, and it is also strongly nonlinear, strongly coupled, and time-varying. Therefore, the essence of accurate control of autonomous underwater robots is the transformation of motion between poses (position and orientation are collectively called poses). The quality of attitude control directly affects the effectiveness of AUVs for specific applications such as tracking, obstacle avoidance, handling, and formation. Proportion Integration Differentiation (PID) control system can reduce the impact [7] of water environment interference and time delay on the accuracy of machine fish attitude control. In this paper, based on the string-level PID algorithm, combined with fuzzy logic control, we designed a hardware control system with STM32F407ZGT6 as the main control chip, combined with a hardware cascade such as a sub-power board and a vision board to form a hardware control system with stable output. The fuzzy PID algorithm [8] is used to model the successful experience accumulated by experts to form a reasonable fuzzy rule table, and the best PID control parameters are obtained after reasoning and practice. After the experimental verification, the error of attitude control is realized to be reduced significantly.

2. Control system

2.1 Hardware of robot control system

The hardware system of the control system includes several major parts such as main control board, vision board, sensor module, etc. STM32F407 as the main control chip can be better applied to motor control, and can be used as a node for sending and receiving data stably and at a lower cost. The Raspberry Pi 4B is equipped with OpenCv to realize image recognition in various environments. Considering the complexity of the patrol algorithm and the convenience of debugging, the hardware system selects the OpenMV vision board to provide the required machine vision for the underwater patrol of the underwater inspection robot.

The underwater inspection robot can use the remote monitoring function of the Raspberry Pi VNC within a certain communication distance [9], so that the operator can observe the underwater situation in real time through the PC. OpenMV vision board also has the function of recording video and extracting real-time data. JY61P attitude sensor is selected, the module integrates high-precision gyroscope

and accelerometer, and the dynamic calculation and Kalman dynamic filtering algorithm are used to quickly solve the current real-time motion attitude of the module. The IIC protocol is used to communicate with the main control MCU, which can solve the current real-time velocity and spatial angle of the robot. MS5803-02BA pressure sensor, the height resolution can reach 20 centimeters water depth. The SPI communication method is used to transfer data between the pressure sensor and the MCU, and the returned pressure value is converted into the height value below the water surface to determine the dive depth of the robot and achieve accurate control.

2.2 Software of robot control system

The underwater inspection robot includes directional inspection and foreign object handling functions. The development environment of the software system is Linux, OpenMV IDE, Keil. The Raspberry Pi is equipped with Linux environment for writing the main camera program and data transfer to MCU, OpenMV IDE is burned into the OpenMV vision board by writing python language for controlling the auxiliary camera, Keil is embedded into the STM32F407 MCU by writing C language program for controlling the total system.

In the process of inspecting pipeline lines, the underwater inspection robot should be able to keep up with the pipeline lines and at the same time keep the distance relative to the pipeline for inspection [10], so that the underwater robot can accurately drive the waterproof servo to turn a certain angle during the inspection process and then make the removal device accurately clean off the foreign objects attached to the pipeline.

The initial setup of the pipeline inspection OpenMV vision board is relatively simple. First, it needs to collect image data including the pipeline, black foreign objects attached to the pipeline and the surrounding environment, and grayscale this image as shown in the Fig. l. If the robot inspection process appears to deviate from the pipeline line condition, and the pipeline is first recognized. The linear regression calculation function img.get_regression() in the OpenMV IDE editor is called, and using this function, the angular deviation and intercept deviation of the robot relative to the pipeline line can be measured.

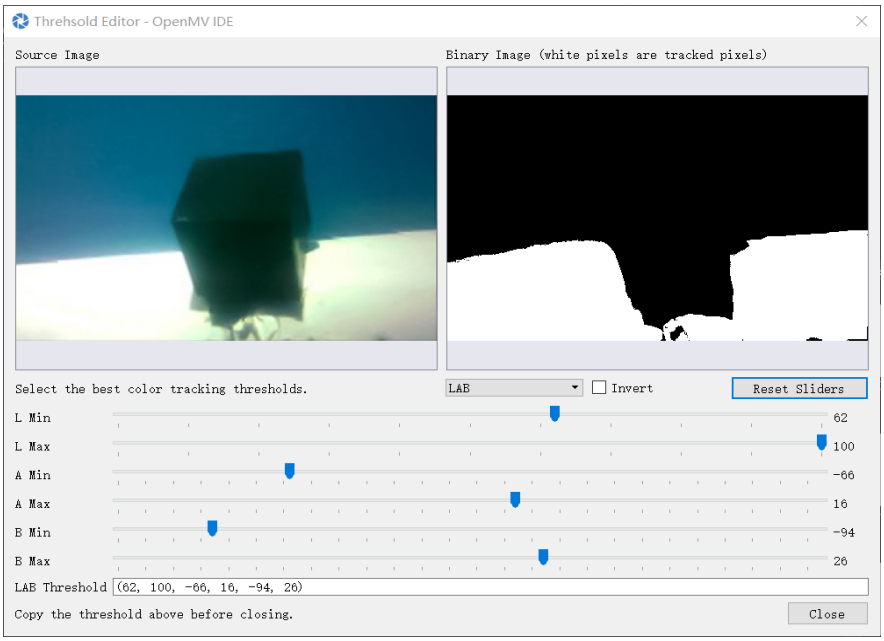

Fig. 1 Threshold processing

When the foreign object handling OpenMV identifies the foreign object attached to the pipeline line, the underwater inspection robot should drive the removal device, which must move quickly and keep the end of the removal mechanism extended for a period of time. In this process, when the foreign object handling vision board identifies the foreign object attached to the pipeline, the robot should precisely realize the grasping action and ensure a stable posture. During the foreign object testing process, black square foreign objects and cylindrical foreign objects were selected for initial program debugging.

3. Attitude control algorithms

3.1 Coordinate system establishment and conversion

For the analysis of the underwater robot attitude control are first to establish the static and dynamic coordinate system with the center of the robot as the origin [11], indicating the dynamic and static coordinate system relative to the position of the center point of the underwater inspection robot is shown in the sub-plan schematic.

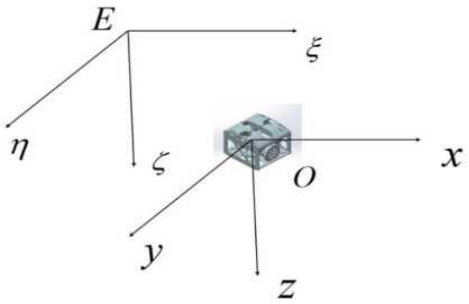

Fig. 2 Schematic diagram of sub-plane

For subsequent calculations, the motion parameters of the robot in the dynamic coordinate system are set symbolically, and the symbolic settings are shown in the table l.

Table 1

Component of motion parameter in dynamic coordinate system

Vector	x	y	z
Speed	u	v	w
Angular velocity	p	q	r
Force	X	Y	Z
Torque	K	M	N

The pose of the robot can be represented by the real-time change condition of the pose angle, which is defined in the table 2.

Table 2

Table 2 Definition of attitude angle in static coordinate system

Rotary shaft	Posture angle	Positive regulations
$E\xi$	Heel angle φ	Clockwise increase around axis
$E\eta$	Pitch angle θ	Increase around the axis up
$E\zeta$	Heading angle ψ	Increase around the axis left

3.2 Force analysis

According to the research on AUV at home and abroad, we can conclude that the force of AUV in water can be divided into propulsive force, static force, hydrodynamic force, and environmental disturbance force. Since we ignore the fluctuation of the water surface caused by natural factors such as wind, the force analysis of the robot does not carry out the relevant calculation of the environmental

disturbance force term. According to the analysis of the main forces on the robot, the resultant force and moment on the robot can be expressed by substituting each force and moment into the following equations.

$$M\dot{v} + C(v)v + D(v)v + g + T + \eta(t) = \tau \quad (1)$$

Compared with underwater robots, the influence of underwater environmental disturbance is negligible. During the actual measurement, the parameters of the control algorithm can be adjusted, so that the robot can well adapt to the small environmental disturbance η(t).

3.2.1 Hydrodynamic force

In most underwater robot research, hydrodynamic force is usually divided into two types, namely viscous hydrodynamic force and inertial hydrodynamic force. When the underwater inspection robot moves, the water flow near the underwater inspection robot will generate movement and exert a certain force on the robot. The force exerted by the surrounding fluid on the robot is usually called hydrodynamic force. These two forces are related to many factors. With the development of the attitude control of underwater robots in recent years, researchers of attitude control of underwater robots at home and abroad usually use the function in the following formula to express the hydrodynamic force of underwater robots.

$$M\dot{v} + C(v)v + D(v)v = f(V, \dot{V}, \Omega, \dot{\Omega}) \quad (2)$$

Under the function formula (2), the hydrodynamic force of the underwater inspection robot is only related to the speed, angular velocity, acceleration, angular acceleration of the underwater inspection robot and the derivatives of these quantities. Therefore, according to the relevant research results or the hydrodynamic coefficient simulation, simplifying the hydrodynamic force of the underwater inspection robot can meet the requirements of analyzing and calculating the force of the underwater inspection robot and solving the attitude control model of the underwater inspection robot.

The viscous hydrodynamic force is the force experienced by the surrounding fluid when the underwater inspection robot moves. When calculating the viscous hydrodynamic force of most underwater robots, we will take into account the symmetry characteristics of the robot structure, and then simplify it. The calculation formula of the viscous hydrodynamic force received by the underwater inspection robot in the subject is: C(v) v + D(v) v.

According to the force analysis formulas for robots at home and abroad, the viscous hydrodynamic force includes linear terms and nonlinear terms. We divide viscous hydrodynamic force into horizontal viscous hydrodynamic force and vertical viscous hydrodynamic force. The viscous hydrodynamic expressions of the horizontal plane and the vertical plane are respectively as follows:

$$\left\{\begin{array}{l} X_V = X_{uu}u^2 + X_{vv}v^2 + X_{rr}r^2 + X_{vr}vr \\ Y_V = Y_v v + Y_r r + Y_{v|v|}v\,|v| + Y_{v|r|}v\,|r| + Y_{r|r|}r\,|r| \\ N_V = N_v v + N_r r + N_{v|v|}v\,|v| + N_{v|r|}v\,|r| + N_{r|r|}r\,|r| \end{array}\right\} \tag{3}$$

$$\left\{\begin{array}{l} X_V = X_{uu}u^2 + X_{ww}w^2 + X_{qq}q^2 + X_{wq}wq \\ Z_V = Z_w w + Z_{|w|}\,|w| + Z_q q + Z_{w|w|}w\,|w| + Z_{|ww|}w^2 \\ + Z_{w|q|}w\,|q| + Z_{q|q|}q\,|q| \\ M_V = M_w w + M_{|w|}w + M_q q + M_{w|w|}w\,|w| + M_{ww}w^2 \\ + M_{w|q|}w^2 + M_{w|q|}w\,|q| + M_{q|q|}q\,|q| \end{array}\right\} \tag{4}$$

The inertial hydrodynamic calculation formula is: $M\dot{v} = -\sum_{j=1}^{6}\lambda_{ij}\left[\dot{V} \quad \dot{\Omega}\right]^T$.

The inertial hydrodynamic coefficient matrix has a total of 36 items, as shown in the following formula:

$$M = \lambda_{ij} = \left\{\begin{array}{cccccc} \lambda_{11} & \lambda_{12} & \lambda_{13} & \lambda_{14} & \lambda_{15} & \lambda_{16} \\ \lambda_{21} & \lambda_{22} & \lambda_{23} & \lambda_{24} & \lambda_{25} & \lambda_{26} \\ \lambda_{31} & \lambda_{32} & \lambda_{33} & \lambda_{34} & \lambda_{35} & \lambda_{36} \\ \lambda_{41} & \lambda_{42} & \lambda_{43} & \lambda_{44} & \lambda_{45} & \lambda_{46} \\ \lambda_{51} & \lambda_{52} & \lambda_{53} & \lambda_{54} & \lambda_{55} & \lambda_{56} \\ \lambda_{61} & \lambda_{62} & \lambda_{63} & \lambda_{64} & \lambda_{65} & \lambda_{66} \end{array}\right\} \tag{5}$$

3.2.2 Static force

The static force mainly includes buoyancy and gravity. The overall design of the underwater inspection robot ensures the design principle of left-right and front-back symmetry. The entire underwater robot is perpendicular to the *xOz* plane and the *yOz* plane, so there is only a distance between the center of gravity and the center of buoyancy whose value is the coordinate difference. The numerical calculations of the static forces are as follows:

$$g=\begin{cases} X_G=(P-G)\sin\theta \\ Y_G=(G-P)\cos\theta\sin\varphi \\ Z_G=(G-P)\cos\theta\cos\varphi \\ K_G=(yG-yP)\cos\theta\cos\varphi-(zG-zP)\cos\theta\sin\varphi \\ M_G=(xG-xP)\cos\theta\cos\varphi+(zG-zP)\sin\theta \\ N_G=(xG-xP)\cos\theta\sin\varphi+(yG-yP)\sin\theta \end{cases} \tag{6}$$

3.2.2 Propulsive force

Considering the overall size of the robot and the size of the selected propeller, the layout of the propeller selected by the robot is shown in the Fig.3.

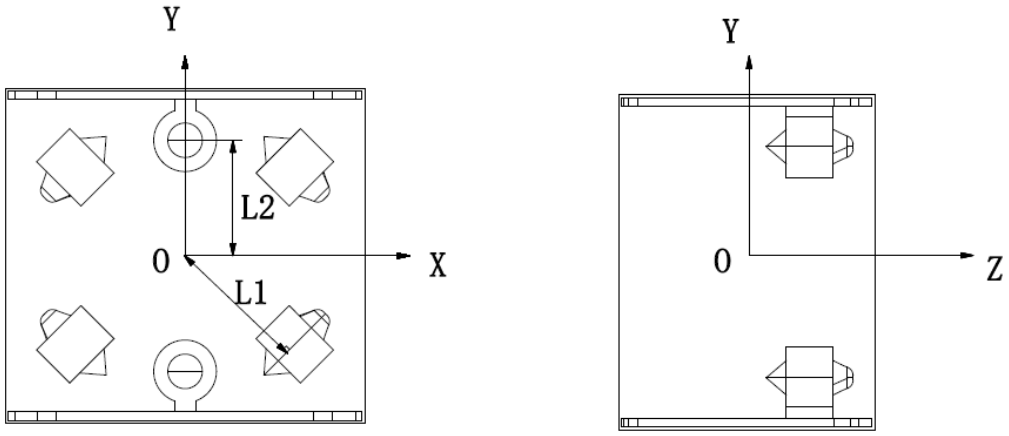

Fig.3 Schematic diagram of the distance between the six thrusters and the center of the robot

$$T=\begin{cases} X_T=T_1\cos\alpha+T_2\cos\alpha \\ Y_T=T_3\cos\alpha+T_4\cos\alpha \\ Z_T=T_5+T_6 \\ K_T=0 \\ M_T=0 \\ N_T=T_1L_1+T_2L_1+T_3L_1+T_4L_1 \end{cases} \tag{7}$$

3.3 Attitude control model

The system transfer function includes the transfer function between the control signal and thrust, the thruster transfer function, and the transfer function between thrust and speed.

3.3.1 Kinetic equations

In and out, traverse, up and down are linear motion, and the equation of linear motion can be obtained according to Newton's second law. R_G is the distance from the center to the far point of the dynamic coordinate system [12].

$$V_G = V + \Omega R_G \tag{8}$$

$$F_{\Sigma} = ma = m\frac{dV_G}{dt} \tag{9}$$

By associating the above two equations with the vector components of each linear motion, the equation for the linear motion of the robot can be obtained as shown in the following equation.

$$\begin{cases} X = m[\dot{u} - vr + wq - x_G(q^2 + r^2) + y_G(pq - \dot{r}) + z_G(pr + \dot{q})] \\ Y = m[\dot{v} - wp + ur - y_G(p^2 + r^2) + z_G(qr - \dot{p}) + x_G(pq + \dot{r})] \\ Z = m[\dot{w} - uq + vp - z_G(p^2 + q^2) + x_G(pr - \dot{q}) + y_G(qr + \dot{p})] \end{cases} \tag{10}$$

Bow, heel and trim are all rotational motions, and the rotational motion equation can be obtained according to the theorem of moment of momentum, where I_0 is the inertia matrix of the robot.

$$M_{\Sigma} = I_0\Omega \tag{11}$$

$$\frac{dM_{\Sigma}}{dt} = \frac{dI_o\Omega}{dt} = M_o - maR_G \tag{12}$$

Since the robot is symmetrical to the face *xOz* and *yOz* the surface in the dynamic coordinate system, the quantities in the inertia matrix other than the diagonal are taken as 0.

$$I_0 = \begin{Bmatrix} I_x & 0 & 0 \\ 0 & I_y & 0 \\ 0 & 0 & I_z \end{Bmatrix} \tag{13}$$

The above three equations are combined with the vector components of each rotational motion, the rotational equation of motion.

$$\begin{cases} K = I_x \dot{p} + (I_z - I_y)qr + m[y_G(\dot{w} + vp - uq) - z_G(\dot{v} + ur - wp)] \\ M = I_y \dot{q} + (I_x - I_z)qr + m[z_G(\dot{u} + wp - vr) - x_G(\dot{w} + vp - uq)] \\ N = I_z \dot{r} + (I_y - I_x)qr + m[x_G(\dot{v} + ur - wp) - y_G(\dot{u} + wp - vr)] \end{cases} \tag{14}$$

The six-degree-of-freedom dynamics equations of the underwater inspection robot can be obtained by substituting all the combined force and combined moment vector equations of the robot into the horizontal and rotational equations of motion and replacing the forces or moments in the horizontal and rotational equations of motion.

Considering that there is a large number of cross-coupling between the equations in the six degrees of freedom dynamics equations, the simplification of the dynamics equations can adopt the more common calculation method at present, that is, when calculating the horizontal plane dynamics equations, the parameters w, p, q, $\dot{w}$, $\dot{p}$, $\dot{q}$ in the horizontal plane dynamics equations that are not related to the horizontal plane motion are taken as 0 to obtain the horizontal plane dynamics equations, and similarly, the vertical plane dynamics equations can be obtained.

The motion attitude controlled by the algorithm is divided into two kinds of attitudes, bow turning and lifting. In the bow turning attitude, let $u = v = \dot{u} = \dot{v} = 0$ and in the elevation attitude, let $u = q = \dot{u} = \dot{q} = \theta = 0$. Therefore, by substituting the bow angle and depth into the equation, we can get the bow turning attitude control equation and elevation attitude control equation as the following two equations respectively, both equations omit the hydrodynamic coefficient which has little effect on the change of the respective attitude angle.

$$(T_1 + T_2 + T_3 + T_4)l_1 = (I_z + \lambda_{66}\ddot{\psi}) - N_r\dot{\psi} \tag{15}$$

$$T_5 + T_6 - \lambda_{33}\ddot{\zeta} + Z_w\dot{\zeta} + (G - P) = m\ddot{\zeta} \tag{16}$$

3.3.2 Control function

The thrust and speed of the factory motor are linearly related, and the relationship between thrust and speed can be replaced by a constant. The transfer function of thrust and speed is usually expressed in the following form.

$$G_{Tn}(s)=\frac{T(s)}{n(s)}=2K_T\rho D^4 n_0 \tag{17}$$

Where K_T is the thrust coefficient of the propeller thruster, ρ is the density of the fluid around it when the robot is moving, D is the propeller diameter of the propeller thruster. K_T depends on the propeller structure of the propeller thruster. The transfer function of the thrust and angle of the bow process is shown in Equation 18. This transfer function involves an inertia-like hydrodynamic coefficient, a viscous-like hydrodynamic coefficient, a length value, and a rotational inertia.

$$G_{\Psi}(s)=\frac{\Psi(s)}{\sum\limits_{i=1,2,3,4} T_i(s)}=\frac{L_1}{(I_Z+\lambda_{66})s^2-N_r s} \tag{18}$$

The transfer function of thrust and depth during lift is shown in equation 19. This transfer function involves an inertia-like parameter, a viscous parameter, and an overall robot mass.

$$G_{\zeta}(s)=\frac{\zeta(s)}{\sum\limits_{i=5,6} T_i(s)-\Delta G(s)}=\frac{1}{(m+\lambda_{33})s^2-Z_W s} \tag{19}$$

Based on the mechanical design of the robot, the literature and finite element analysis, the parameters of the two posture control functions can be derived.

3.4 Fuzzy PID control

The fuzzy PID controller is an adaptive control system that regulates the control parameters of a digital PID control system by means of fuzzy control. It includes fuzzy inference and conventional PID control parts. Input deviation and its rate of change, then achieve synchronous parameter correction by fuzzy control rules.

Among the important fuzzy rules in fuzzy PID as shown in the table 3, 4, the solution fuzzy formula is $V_o=\frac{\sum\limits_{i=0}^{n} M_i * F}{\sum\limits_{i=0}^{n} M_i}$, where M is the degree of affiliation, F is the fuzzy quantization value; in fact, because of the nature of the affiliation function used, the sum of the membership degrees calculated in any direction is 1,

so the denominator can be omitted. So the calculation of each object is actually a matrix operation, the formula is $K=[M_{e1} \quad M_{e2}]\begin{bmatrix} F_a & F_b \\ F_c & F_d \end{bmatrix}[M_{e1} \quad M_{e2}]^T$; if you are using quantized values, you also need to convert to actual values, or you can use physical values directly. Which type of parameter value to use needs to be determined according to the actual situation. After getting the increment, coefficients can also be introduced to enlarge and reduce the amount of Kp, Ki and Kd change, the specific implementation formula is $K(n)=K(n-1)+\Delta K^{*}\alpha$, where ΔK is the calculated value obtained, and α is the coefficient that sets the impact of the increment on the final value.

Table 3

Kp rule fuzzy design table

ΔKp	Negative Large	Negative Medium	Negative Small	Zero	Positive Small	Positive Medium	Positive Large
Negative Large	Positive Large	Positive Large	Positive Medium	Positive Medium	Positive Small	Zero	Zero
Negative Medium	Positive Large	Positive Large	Positive Medium	Positive Medium	Positive Small	Zero	Negative Small
Negative Small	Positive Medium	Positive Medium	Positive Medium	Positive Small	Zero	Negative Small	Negative Small
Zero	Positive Medium	Positive Medium	Positive Small	Zero	Negative Small	Negative Medium	Negative Medium
Positive Small	Positive Small	Positive Small	Zero	Negative Small	Negative Small	Negative Medium	Negative Medium
Positive Medium	Positive Small	Zero	Negative Small	Negative Medium	Negative Medium	Negative Medium	Negative Large
Positive Large	Zero	Zero	Negative Medium	Negative Medium	Negative Medium	Negative Large	Negative Large

Table 4

Ki rules fuzzy design table

ΔKi	Negative Large	Negative Medium	Negative Small	Zero	Positive Small	Positive Medium	Positive Large
Negative Large	Negative Large	Negative Large	Negative Medium	Negative Medium	Negative Small	Zero	Zero
Negative Medium	Negative Large	Negative Large	Negative Medium	Negative Small	Negative Small	Zero	Zero
Negative Small	Negative Large	Negative Medium	Negative Small	Positive Small	Zero	Positive Small	Positive Small
Zero	Negative Medium	Negative Medium	Negative Small	Zero	Positive Small	Positive Medium	Positive Medium
Positive Small	Negative Medium	Negative Small	Zero	Positive Small	Negative Small	Positive Medium	Positive Large

Positive Medium	Zero	Zero	Positive Small	Positive Small	Positive Medium	Positive Large	Positive Large
Positive Large	Zero	Zero	Positive Small	Positive Medium	Positive Medium	Positive Large	Positive Large

4. Experiment analysis

The experiment was conducted with the robot arm sinusoidal motion as the object, and then the experiment was conducted with the AUV hovering operation, that is to say, the AUV's own position was fixed and motionless, and the robot arm on it did the extension motion, and the experimental data were analyzed.

4.1 Data Analysis of Sinusoidal Motion of Robotic Arm Joints

From the Fig.4 analysis, it can be seen that the mean variance of the AUV longitudinal attitude angle under conventional PID control is 16.84°, while the mean variance of the longitudinal attitude angle under fuzzy PID control is 9.55°, and its value decreases by 43.29%. The maximum absolute and average absolute values were 8.09°, 0.86° and 5.94°, 0.25°, respectively, with a decrease of 26.58% and 70.93%, respectively. Compared with the conventional PID control, the mean square error, mean absolute error and maximum absolute error of the longitudinal tilt attitude angle error decreased by 28.75%, 36.96% and 37.48%, respectively, for fuzzy PID. The above data show that the control effect of longitudinal tilt attitude based on fuzzy PID during the motion of the robot arm is better than that of conventional PID control.

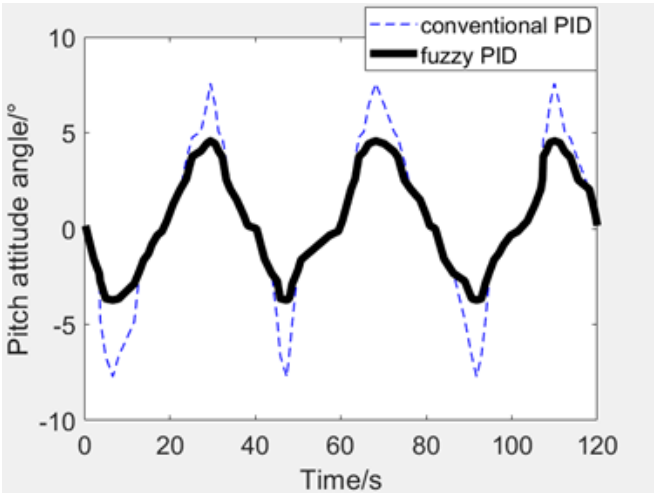

Fig. 4 Pitch attitude angle curve

The 5 analysis of the graph shows that the mean variance of the AUV transverse tilt attitude angle under conventional PID control is 15.55°, while the mean variance of the longitudinal tilt attitude angle under fuzzy PID control is 5.83°, and their values have decreased by 62.50%. Their mean absolute values were 0.73° and 0.44°, which decreased by 65.90%; their maximum absolute values were 7.32° and 4.59°, which decreased by 37.30%. The analysis of the graph 6 shows that the mean variance, mean absolute error, and maximum absolute error of the longitudinal tilt attitude angle error decreased by 52.33%, 68.66%, and 76.80%. The above data show that the control effect of the longitudinal tilt attitude based on fuzzy PID in the motion of the robot arm is better than the conventional PID control.

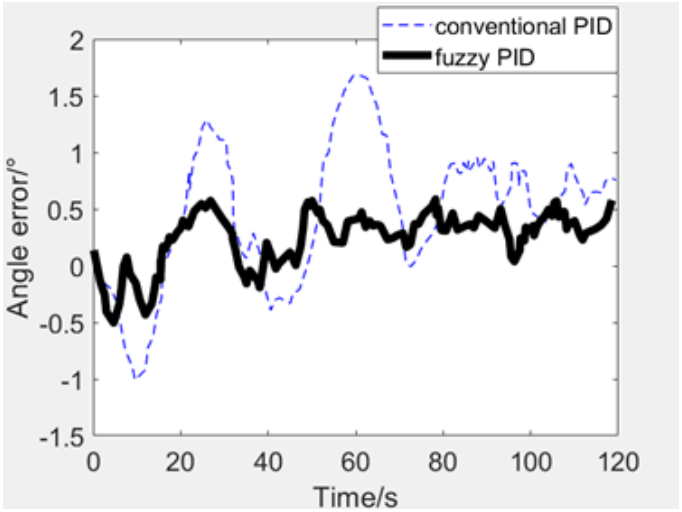

Fig.5 Angle error

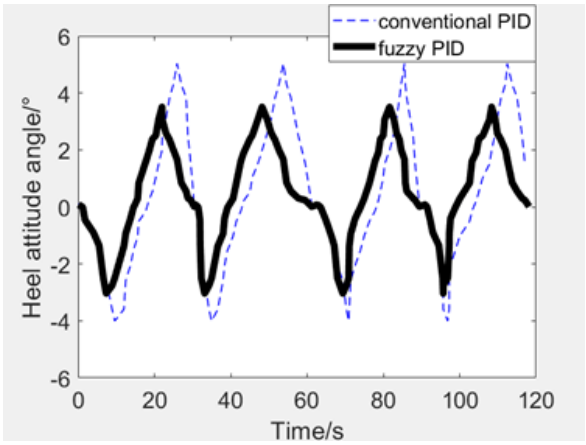

Fig. 6 Heel attitude angle curve

4.2 Data analysis of hover operation

From Fig.7 the experimental results, it can be seen that under the conventional PID control condition, the longitudinal tilt attitude angle of AUV carrier is maximum at 16s with the maximum value of 0.52°, and reaches the maximum negative angle at about 38s with the value of -2.68°, after which the attitude angle starts to recover to 0° slowly and reaches near 0° at 75s. Under the fuzzy PID condition, the longitudinal tilt attitude angle of the AUV carrier is maximum at 8s with a maximum value of 0.51°, and reaches the maximum negative angle at 34s with a value of -3.98°, and reaches near 0° at 115s. The maximum absolute value of the fuzzy PID is reduced by 32.66% compared to the conventional PID.

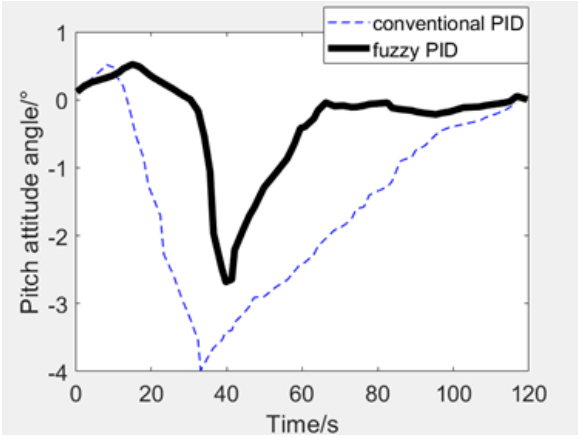

Fig. 7 Pitch attitude angle curve

From the experimental results of the Fig.8, it can be seen that the transverse tilt attitude angle is first increasing and then decreasing, and finally tends to be near 0°. Under the PID control condition, the AUV carrier occurs transverse tilt attitude angle reaches the maximum at 39s with the maximum value of -1.85°, after which the attitude angle starts to slowly recover to 0° and reaches near 0° at 90s, after which it starts to oscillate. Under the fuzzy PID condition, the AUV carrier tilted sideways with the maximum attitude angle of -1.65° at 22s and reached near 0° at 80s, and then stabilized. The maximum absolute value of the fuzzy PID is reduced by 43.24% compared with the conventional PID.

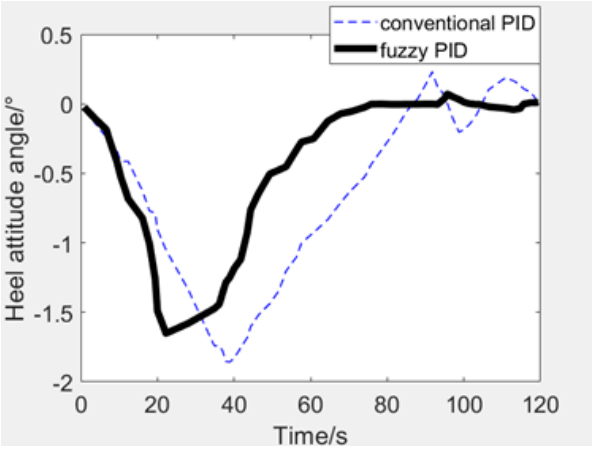

Fig. 8 Heel attitude angle curve

5. Conclusions

Based on the fuzzy PID attitude control system to control six thrusters respectively, it can achieve relatively small steady-state error and relatively stable motion attitude, and resist the influence of certain surge. The attitude is corrected in real time in the pipeline patrol scenario to ensure that the visual recognition module can be aligned with the pipeline, and can cope with the stable situation even when encountering 90° steering scenarios. The experiment verifies that the lateral and longitudinal attitude angle error is reduced by more than 50% compared with the traditional solution in the motion state, and the error angle reduction in the stationary suspension state is erased by more than 30%. The results of simulation and physical experiments show that the fuzzy adaptive cascade PID algorithm can adjust the proportional, integral and differential coefficient parameters of the inner loop of the cascade PID algorithm online, which solves the problem of weak environmental adaptability of the fixed inner loop coefficients. Based on the fuzzy adaptive string-level PID algorithm of the robot to reach the target position improves the control accuracy while accelerating the response speed, and can effectively avoid the AUV directional angle jump, with strong robustness and good stability, and higher application value. Follow-up work can add attitude sensors to the hardware structure of AUV to verify the feasibility of image processing to provide real- time attitude and achieve more accurate attitude control of AUV.

Acknowledgement

Fund project: Fundamental Research Funds for Central Universities (2572017CB08).

REFERENCES

[1]. *J. Gadelho, J.M Rodrigues., A. Lavrov, et al*. "Heave and sway hydrodynamic coefficients of ship hull sections in deep and shallow water using Navier-Stokes equations", Ocean Engineering, **vol. 154**, 2018, pp. 262-276.

[2]. *T. Prestero.* "Verification of a six-degree of freedom simulation model for the remus autonomous underwater vehicle", Boston: Massa-chusetts Institute of Technology and Woods Hole Oceanographic Institution, 2001.

[3]. *Y. Huang, Y. Li, J.C. Yu, et al.* "Status and development trend of AUV intelligence", Robotics, **vol. 42**, no. 2, 2020, pp. 215-231.

[4]. *S. McPhail, M. Furlong, V. Huvenne, et al.* "Autosub6000: Its first deepwater trials and science missions", Underwater Technology, **vol. 28**, no. 3, 2009, pp. 91-98.

[5]. *Ura T, Obara T, Nagahashi K, et al.* Introduction to an AUV "r2D4" and its Kuroshima Knoll survey mission//Oceans Piscataway, USA: IEEE, 2004, pp. 840-845.

[6]. *Yun LIU, Yong JIANG*, "Kinematics Analysis and Experimental Research of Deep Sea Mining Robot," UPB Scientific Bulletin, Series D: Mechanical Engineering, **vol. 83**, 2021, pp. 4-18.

[7]. *Y.J. Song, G. Wang, W.S. Tang, Q. Zhao.* "Fuzzy adaptive cascade PID-based positional control of machine fish. Control Engineering", https://doi.org/10.14107/j.cnki.kzgc.20210576

[8]. *S. Zhang, J.J. Xiao.* "A review of underwater vector propulsion researcher", Ship Science and Technology, **vol. 41**, no. 07, 2019, pp. 5-9.

[9]. *W. Zhen.* "Research on hydrodynamic modeling and motion control of cable-controlled underwater robot", Shandong: Shandong University, 2019.

[10]. *Y.T. Ma, R. Zheng, B. Yu.* "Stability control of autonomous underwater robots with transitional target values of nonlinear PID for variable depth motion", Control Theory and Applications. **vol. 35**, no. 8, 2018, pp. 1120-1125

[11]. *J.H. Yang, S.Y. Tian.* "Research on sliding mode theory based underwater robot fixed depth control algorithm", Computer Measurement and Control, **vol. 25**, no. 08, 2017, pp. 43-45+57.

[12]. *J. Sverdrup-Thygeson, E. Kelasidi, K.Y. Pettersen, J.T. Gravdahl.* "Modeling of underwater swimming manipulators", IFAC-PapersOnLine, **vol. 49**, no. 23, 2016, pp. 81-88.